TEAM MEMBERS:

SWEEKRITHI SHETTY
NATASHA MATHIAS
FARHEEN SHAIKH
CHIRAYU THAKUR

SUPERVISORS:

SATISH CHAVAN
RAJBABU VELMURUGAN
ANIL KOTTANTHARAYIL

Detection of Micro-Cracks in Electroluminescence Images of Photovoltaic Modules

Abstract

This paper presents detection of micro-cracks in solar cells using Electroluminescence (EL) images. The preprocessing step in this work involved separation of solar panel section from background of EL image, use of perspective transformation, and separating individual solar cells from the Photovoltaic (PV) panel. Discrete Wavelet Transform (DWT) and Stationary Wavelet Transform (SWT) are used to extract textural features from these solar cells. These features were then used for classification of solar cells into cracked and non-cracked cells using Support Vector Machine (SVM) and Back Propagation Neural Network (BPNN). The networks were trained with a dataset of 2000 EL images and tested with a dataset of 300 test images. The percentage classification accuracy obtained is 92.67% and 93.67% using SVM and BPNN, respectively.

Keywords:

Micro-crack in Solar Cells, Electroluminescence Image, Perspective Transformation, Support Vector Machine, Back Propagation Neural Network.

1. Introduction

Depleting energy resources and huge demand for renewable energy has led to an increase in the demand of solar cells which are a major component of Photovoltaic (PV) modules [1]. As a result, the manufacturing of solar cells has increased in recent years. The growth of solar market will reach 14% in 2020 with generation of energy in the range 121-154GW [2]. Multi-crystalline cells constitute revenue of more than 50% of the world production of solar energy [1]. Solar cells are manufactured as monocrystalline and polycrystalline depending upon manufacturing material. Monocrystalline modules have a higher efficiency compared to polycrystalline modules. However, solar cells with polycrystalline silicon are manufactured on large scale due to cheaper manufacturing and processing expenses. This provides opportunities for automation in this industry. Even though many operations have been automated, the inspection and grading process of PV modules continues to be done manually or semi-manually. The presence of micro-cracks in solar cells has an adverse effect on the reliability of the PV module. Visual analysis of evaluating solar cells for defects, is costly and a time consuming task. Therefore, use of EL images for evaluating the quality of PV modules is a faster and cheaper solution.

This paper deals with automatic segmentation of solar cells and classifies them into cracked/non-cracked ones.

2. Literature Survey

Automatic solar cell segmentation from EL images using edge features was proposed by Deitsch et al. [3]. Dhimish et al. measured the power loss due to micro cracks on PV module which has significant impact on effective power performance and production of energy [4, 5]. Gou et al. presented the adverse effect of microcracked length and area on power throughput along with safety hazards [20]. Use of anisotropic diffusion filtering was done for microcrack detection in polycrystalline cells [1]. Tsai et al. used EL images of polycrystalline PV module to identify defects in solar cells using Fourier image reconstruction [16]. Independent Component Analysis (ICA) approach was for detection of cracks in solar cells with an accuracy of 93.40% [17]. Finger interruptions were detected from monocrystalline solar cells using binary clustering of features [18]. Abdelhamid et al. analysed various reasons for the micro-cracks in monocrystaline and polycrystalline solar cells [19].

3. Proposed Methodology

The proposed system utilizes EL images as an input to provide information about the quality of solar cell. The block schematic of this system for detection of micro-cracks is shown in Fig. 1.

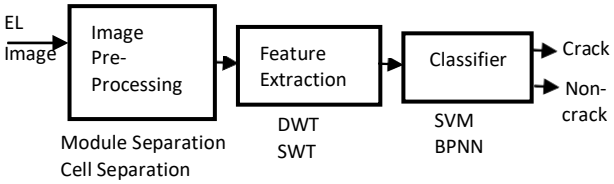

Figure 1: Detection of micro-cracks in EL images of PV module.

Crack Detection in mono crystalline modules is a relatively straightforward procedure; however in poly crystalline modules the presence of grain boundaries which are an intrinsic defect and appear as dark patches having similar gray level intensities as micro-cracks complicates the detection of micro-cracks. In spite of this difficulty, their identification is still possible because micro-cracks are visible as prominent lines having low gray level intensity and high gradient [6].

a) Suppressing fingers and busbars:

Fingers and busbars are more prominent in EL images of polycrystalline cells compared to monocrystalline cells [18]. Fingers occur at periodic intervals in the cell and are perpendicular to the busbars. Due to inhomogeneous illumination of the CCD sensor, it is observed that intensity distribution is not uniform within a cell and between the cells of a module. Broken fingers as well as non-uniform illumination of the module directly affect the analysis of microcracks in the solar cell [1]. The solution is to remove the periodic interruption of fingers and reduce the non-uniformity in the illumination of the module. Suppressing fingers and busbars using frequency domain filter is as shown in Fig. 2.

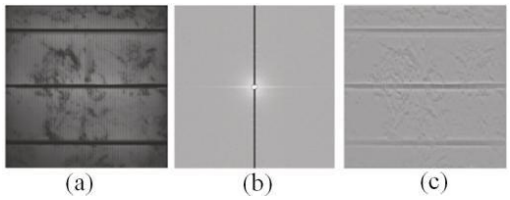

Figure 2: Suppressing fingers and bus bars using ring filter: (a) Original EL image (b) Fourier spectrum after implementing filter (c) Filtered EL image

b) PV Module Separation:

In order to extract solar cells from EL images of solar panel, detection of the four corners of the PV module is essential [6]. Automatic corner detection is obtained by perspective transformation and shear matrix through a template image. Assuming that the image intensity of the PV module varies with different angles of view due to variation in focal-length, rotation and tilt, the image is multiplied by a tilt factor before applying the perspective warp.

The PV module is extracted from the background and straightened using perspective transformation as shown in Fig. 3 using the following algorithm:

a) Select largest contour:

1. Converting image into binary image using thresholding operation.
2. Find the contours in the binary image.
3. Arrange the contours in descending order.
4. Choose the largest contour which has no. of sides approximately equal to 4.

b) Estimate the four corner pixels.

c) Compute height and width of the new image.

d) Obtain perspective transform matrix to straighten the PV module.

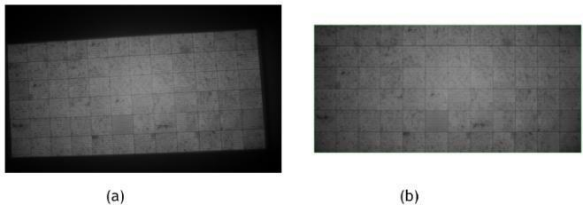

Figure 3: Module Separation: (a) Original EL Image (b) EL Image after module separation and perspective transformation

Fig. 4: Morphological Closing Operation: a) Result image using vertical structuring element b) Result image using horizontal structuring element

c) Solar Cell Separation

The cell separation algorithm for automatically separating the solar cells is as follows:

1. The perspective corrected image is used as input image for this module.
2. Apply adaptive histogram equalization on the image.
3. Apply closing operation on resultant image to generate two images using vertical and horizontal lines as structuring elements. A closing with vertical lines will remove all horizontal lines and a closing with horizontal lines will remove all vertical lines as shown in Fig. 4.
4. Compute sum along each row for Fig. 4(a) and column for Fig. 4(b).
5. The local minima corresponding to rows and columns are the boundaries of cells in the panel (Fig. 5)
6. Detect and find coordinates of corners using Harris Corner Detection (Fig. 6)
7. Crop each cell using the coordinates of detected corners (Fig. 7).

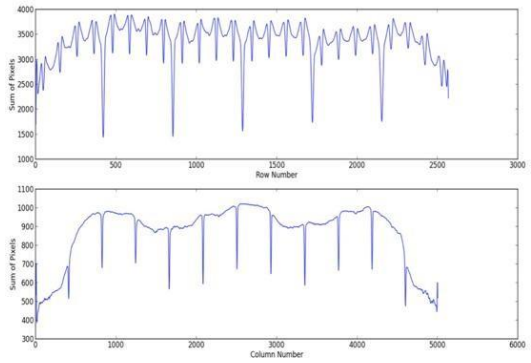

Figure 5: Sum of pixel intensities along rows and columns. Local minima determines cell boundary.

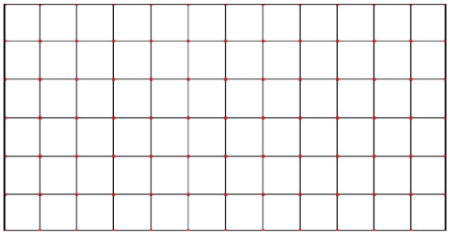

Figure 6: Harris Corner Detection

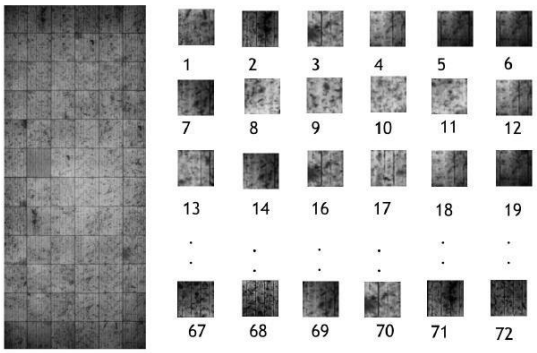

(a) (b)

Figure 7: Cell Separation (a) Original EL image (b) Separated Solar Cells.

d) Feature Extraction

In this work, Discrete Wavelet Transform (DWT) and Stationary Wavelet Transform (SWT) are used to extract textural and edge features from solar cells.

i. Discrete Wavelet Transform (DWT)

Discrete Wavelet Transform (DWT) extracts features very efficiently in different frequency spectra [7]. It models textural and edge information separately. The wavelet function, ψ(t) is defined as in (1).

$$\psi_{a,b}(t) = \frac{1}{\sqrt{a}}\psi\left(\frac{t-a}{b}\right) \quad (1)$$

Here, ψ(t) is mother wavelet. Translation factor „a" and dilation factor „b" are used to capture information in varying scales and spectra.

2D DWT decomposition provides information in four bands as one approximation sub-band and three edge subbands. The decomposition process can be iterated with successive „approximation subband" resulting in various levels of resolutions. DWT wavelet decomposition is as shown in Figure 8. Here, „*S*" and „*D*" refer to the coefficients of the approximation plane and the detailed components, respectively. „*h*" and „*g*" are the low-pass filter and high-pass filter coefficients, respectively.

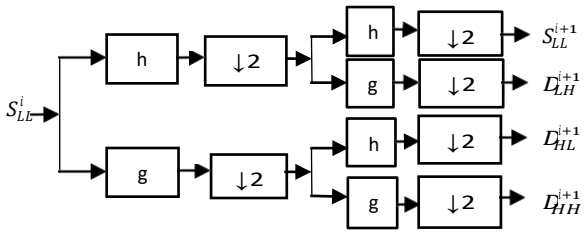

Figure 8: DWT Decomposition

In this paper, four levels of decomposition using DWT are implemented to obtain 13 sub-bands. Following features are extracted using these sub-bands [8]:

1. $Mean = \frac{1}{N^2}\sum_{i,j=1}^{N} p(i,j)$
   Where, $p(i,j)$ is the image value at (i,j).
2. Min= $Min[p(i,j)]$
3. Max= $Max[p(i,j)]$
4. $\text{Variance} = \frac{1}{N-1}\sum_{i,j=1}^{N} |p\,i,j - \text{Mean}|^2$
5. Max. Energy= $(Max[p(i,j)])^2$
6. $\text{Std. Dev.} = \frac{1}{N^2}\sum_{i,j=1}^{N}[p\,i,j - \text{Mean}]^2$
7. $\text{Entropy} = -\sum_{i,j=1}^{N} p\,i,j \log_2(p\,i,j)$
8. $Kurtosis = \frac{\frac{1}{N}\sum_{i,j=1}^{N}(p\,i,j - \text{Mean})^4}{\left(\frac{1}{N}\sum_{i,j=1}^{N}(p\,i,j - \text{Mean})^2\right)^2}$
9. $Skewness = \frac{\frac{1}{N}\sum_{i,j=1}^{N}(p\,i,j - \text{Mean})^3}{\left(\frac{1}{N}\sum_{i,j=1}^{N}(p\,i,j - \text{Mean})^2\right)^{\frac{3}{2}}}$

ii. Stationary Wavelet Transform (SWT)

The decomposition process of Stationary Wavelet Transform (SWT) is similar to DWT except the down-sampling process [9, 10]. SWT has advantage over DWT in shift invariant signal representation [11]. Like DWT, four decomposition levels are obtained using SWT to get 13 sub-bands. The size of these sub-bands is same as that of the original image as shown in Figure 9.

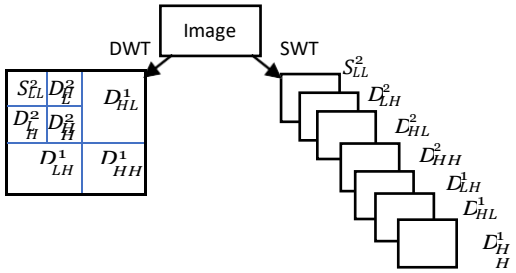

Figure 9: Image decompositions for DWT and SWT

Apart from the features extracted using DWT, a few other features are also extracted using SWT.

- Max= *Max*[*C*(*i*,*j*)]
  Where, *C*(*i*,*j*) denotes value at (*i*,*j*) in covariance matrix
- Min= *Min*[*C*(*i*,*j*)]
- Entropy = $-\sum_{i,j=1}^{N} C(i,j)\log_2(C(i,j))$
- Energy = $\sum_{i,j=1}^{N} C^2(i,j)$
- Maximum Probability= *Max*[*C*(*i*,*j*)]
- Homogeneity = $\sum_{i,j=1}^{N} (1+(1-j)^2)^{-1}$ (a)

e) Classification:

Two classifiers, Support Vector Machine (SVM) [11, 12, 13] and Back Propagation Neural Network (BPNN) [14] are used in this work. Both the methods are supervised learning techniques wherein targets need to be provided for learning.

SVM classifier was implemented using a linear kernel. The value of cost function, *C* was determined and its value tested by using 5-fold cross validation technique. In this validation, the training set was first partitioned into 5 subsets. Each subset was tested sequentially using the SVM which was trained on the remaining subsets. Thus, five different accuracies were obtained. Cross-validation for identifying a good value of *C* helps in avoiding the problem of over fitting.

Back propagation learning algorithm was used in similar way to feed forward network in which the error generated during the forward path is propagated back to hidden layers. At the output layer, the test image was evaluated for existence of any cracks.

4. Results and Discussion

The training dataset contains 2000 images and the testing dataset contains 300 images. Distribution of cracked and non-cracked cells is given in Table 1.

The sample normal solar cells and cracked cell are presented in Figure 10. The parameters like accuracy, sensitivity and specificity are used to evaluate the performance of methods used for feature extraction and classifiers. These parameters are calculated using the equations (2)-(4) [15].

Here, TP denotes the number of cracked cells accurately detected, TN is the number of normal cells detected as normal, FP gives number of normal cells detected as cracked, and FN is cracked cells detected as normal cells.

$$Accuracy = \frac{TP+TN}{TP+TN+FP+FN} \quad (2)$$

$$\text{Sensitivity} = \frac{TP}{TP+TN} \quad (3)$$

$$\text{Specificity} = \frac{FP}{FP+FN} \quad (4)$$

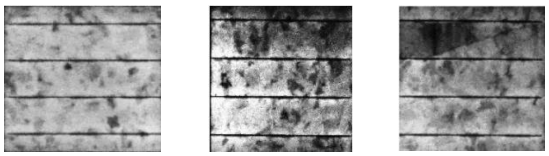

Figure 10: Sample Solar Cells: (a) and (b) Normal Cells (c) Cracked Cell

Table 1: Distribution of Cracked and Non-Cracked Cells in Dataset

Dataset	Cracked Cells	Non-Cracked Cells	Total
Training	1000	1000	2000
Testing	150	150	300

Table 2: Classification Results of Test Set

Classifier	Accuracy (%)	Sensitivity (%)	Specificity (%)
SVM	92.67	93.33	92.00
BPNN	93.67	100.00	87.33

Table 2 presents the performance of two classifiers, SVM and BPNN for feature extraction based on DWT and SWT. Classification accuracy of 92.67% and 93.67% is obtained using SVM and BPNN, respectively. The confusion matrix is given in Fig. 11. It is observed that the accuracy and sensitivity of BPNN is better than that of SVM. However, specificity of SVM is better than BPNN.

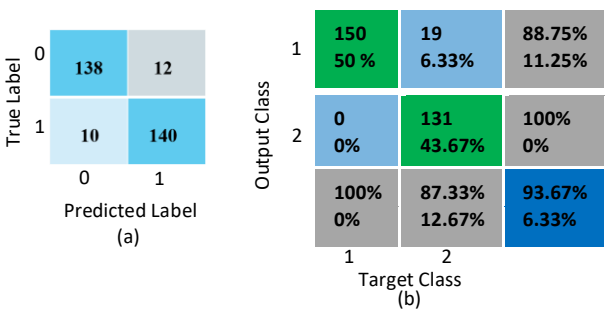

Figure 11: Confusion matrix for DWT feature vector with classifier as (a) SVM and (b) BPNN

5. Conclusion

In this paper, automatic detection and classification of micro-cracks in EL images of PV solar panels is proposed. The textural and edge based features of solar cells are extracted using DWT and SWT and used for classification using SVM and BPNN. As BPNN is the best tool for non-linear data classification, it outperforms SVM for the classification.

References

[1] Said Amirul Anwar and Mohd Zaid Abdullah, "Micro-crack detection of multicrystalline solar cells featuring an improved anisotropic diffusion filter and image segmentation technique," *EURASIP Journal on Image and Video Processing*, Article no.15, 2014.

[2] Angus McCrone, "Energy, Vehicles, Sustainability – 10 Predictions for 2020," BloombergNEF, 16 January 2020.

[3] Sergiu Deitsch, Claudia Buerhop-Lutz, Andreas Maier, Florian Gallwitz, Christian Riess, "Automatic classification of defective photovoltaic module cells in electroluminescence images," *Solar Energy*, vol. 185, pp. 455-468, 2019.

[4] M. Kntges, I. Kunze, S. Kajari-Schrder, X. Breitenmoser, and B. Bjrneklett, "The risk of power loss in crystalline silicon based photovoltaic modules due to micro-cracks," *Solar Energy Materials and Solar Cells*, vol. 95, no. 4, pp. 1131-1137, 2011.

[5] M. Dhimish, V. Holmes, M. Dales and B. Mehrdadi, "Effect of micro cracks on photovoltaic output power: case study based on real time long term data measurements," *In Micro & Nano Letters*, vol. 12, no. 10, pp. 803-807, 2017.

[6] K. G. Bedrich, M. Bliss, T. R. Betts, and R. Gottschalg, "Electroluminescence imaging of PV devices: Determining the image quality," *IEEE 42nd Photovoltaic Specialist Conference (PVSC)*, pp. 1–5, 2015.

[7] Chavan, Satishkumar S., and Sanjay N. Talbar, "Multimodality image fusion in frequency domain for radiation therapy," *International Conference on Medical Imaging, m-Health and Emerging Communication Systems (MedCom)*, IEEE, 2014.

[8] Yan Qiu Chen, Mark S. Nixon, and David W. Thomas, "Statistical geometrical features for texture classification," *Pattern Recognition*, vol. 28, no. 4, pp. 537 – 552, 1995.

[9] Chavan, Satishkumar S., et al. "Nonsubsampled rotated complex wavelet transform (NSRCxWT) for medical image fusion related to clinical aspects in neurocysticercosis," *Computers in biology and medicine*, vol. 81, pp. 64-78, 2017.

[10] Satishkumar Chavan, Abhijit Pawar, and Sanjay Talbar, "Multimodality Medical Image Fusion using Rotated Wavelet Transform," *International Conference on Communication and Signal Processing (ICCASP-2016), Advances in Intelligent Systems Research*, vol. 137, pp. 627-635, 2016.

[11] S. Sidhu and K. Raahemifar, "Texture classification using wavelet transform and support vector machines," *Canadian Conference on Electrical and Computer Engineering*, pp. 941–944, 2005.

[12] Shutao Li, James T. Kwok, Hailong Zhu, and Yaonan Wang, "Texture classification using the support vector machines", *Pattern Recognition*, Vol. 36, no. 12, pp. 2883 – 2893, 2003.

[13] Chih-Wei Hsu, Chih-Chung Chang, and Chih-Jen Lin, "A Practical Guide to Support Vector Classification," *National Taiwan University*, Taipei 106, Taiwan, pp. 1-16, 2016.

[14] Mirza Cilimkovic, "Neural Networks and Back Propagation Algorithm," *Institute of Technology Blanchardstown*, Dublin, Ireland, 2015.

[15] Alireza Baratloo, Mostafa Hosseini, Ahmed Negida, and Gehad El Ashal, "Part 1: Simple definition and calculation of accuracy, sensitivity and specificity," *Emergency*, vol. 3, no. 2, pp. 48–49, 2015.

[16] D. M. Tsai, S.C. Wu, W.C. Li, "Defect detection of solar cells in electroluminescence images using Fourier image reconstruction," *Solar Energy Materials and Solar Cells*, vol. 99, pp. 250–262, 2012.

[17] D. M. Tsai, S. C. Wu, W. Y. Chiu, "Defect detection in solar modules using ICA basis images," *IEEE Transactions on Industrial Informatics*, vol. 9, pp. 122–131, 2013.

[18] D. C. Tseng, Y. S. Liu, C. M. Chou, "Automatic finger interruption detection in electroluminescence images of multicrystalline solar cells," *Mathematical Problems in Engineering*, 2015.

[19] Mahmoud Abdelhamid, Rajendra Singh, Mohammed A Omar, "Review of Microcrack Detection Techniques for Silicon Solar Cells," *IEEE Journal of Photovoltaics*, vol. 4, no. 1, pp. 514-524, 2014.

[20] Xianfang Gou, Xiaoyan Li, Shaoliang Wang, Hao Zhuang, Xixi Huang, and Likai Jiang, "The Effect of Microcrack Length in Silicon Cells on the Potential Induced Degradation Behavior," *Hindawi International Journal of Photoenergy*, Article ID 4381579, pages 6, 2018.